A&A 547, A109 (2012)
DOI: 10.1051/0004-6361/201220031

Astronomy & Astrophysics

Spectroscopy of horizontal branch stars in ω Centauri[⋆,⋆⋆]

C. Moni Bidin[1], S. Villanova[1], G. Piotto[2,3], S. Moehler[4], S. Cassisi[5], and Y. Momany[3,6]

[1] Departamento de Astronomía, Universidad de Concepción, Casilla 160-C, Concepción, Chile
e-mail: cmbidin@astro-udec.cl
[2] Dipartimento di Fisica e Astronomia "Galileo Galilei", Università di Padova, Vicolo dell'Osservatorio 3, 35122 Padova, Italy
[3] INAF – Osservatorio Astronomico di Padova, Vicolo dell'Osservatorio 5, 35122 Padova, Italy
[4] European Southern Observatory, Karl-Schwarzschild-Str. 2, 85784 Garching, Germany
[5] INAF Osservatorio Astronomico di Collurania, via Mentore Maggini, 64100 Teramo, Italy
[6] European Southern Observatory, Alonso de Cordova 3107, Vitacura, Santiago, Chile

Received 17 July 2012 / Accepted 17 September 2012

ABSTRACT

Aims. We analyze the reddening, surface helium abundance and spectroscopic mass of 115 blue horizontal branch (HB) and blue hook (BH) stars in ω Centauri, spanning the cluster HB from the blue edge of the instability strip ($T_{\rm eff}$ = 8000 K) to BH objects with $T_{\rm eff} \approx 50\,000$ K.

Methods. The temperatures, gravities, and surface helium abundances were measured on low-resolution spectra fitting the Balmer and helium lines with a grid of synthetic spectra. From these parameters, the mass and reddening were estimated.

Results. The mean cluster reddening is $E(B-V) = 0.115 \pm 0.004$, in good agreement with previous estimates, but we evidence a pattern of differential reddening in the cluster area. The stars in the western half are more reddened than in the southwest quadrant by 0.03−0.04 mag. We find that the helium abundances measured on low-resolution spectra are systematically higher by 0.20−0.25 dex than the measurements based on higher resolution. No difference in surface helium abundance is detected between HB stars in ω Centauri and in three comparison clusters, and the stars in the range 11 500−20 000 K follow a trend with temperature, which probably reflects a variable efficiency of the diffusion processes. There is mild evidence that two families of extreme HB (EHB) cluster stars ($T_{\rm eff} \geq 20\,000$ K) could exist, as observed in the field, with ∼15% of the objects being helium depleted by a factor of ten with respect to the main population. The distribution of helium abundance above 30 000 K is bimodal, but we detect a fraction of He-poor objects lower than previous investigations. The observations are consistent with these being stars evolving off the HB. Their spatial distribution is not uniform across the cluster, but this asymmetric distribution is only marginally significative. We also find that EHB stars with anomalously high spectroscopic mass could be present in ω Centauri, as previously found in other clusters. The derived temperature-color relation reveals that the HB stars hotter than ∼11 000 K are fainter than the expectations of the canonical models in the U band, while no anomaly is detected in B and V. This behavior, not observed in NGC 6752, is a new peculiarity of ω Centauri HB stars. More investigation is needed to reach a full comprehension of this complex observational picture.

Key words. stars: atmospheres – stars: fundamental parameters – stars: abundances – globular clusters: individual: omega Centauri – stars: horizontal-branch

1. Introduction

Horizontal branch (HB) stars in Galactic globular clusters (GCs) are old stars of low initial mass (0.7−0.9 $M_\odot$) that, after the exhaustion of hydrogen in the stellar core and the ascension along the red giant branch, finally ignite He burning in the core (Hoyle & Schwarzschild 1955; Faulkner 1966). Despite this general comprehension, our knowledge of cluster HB stars still presents many grey areas (see Catelan 2009, for a recent review). In particular, recent observations of HB stars hotter than 20 000 K (extreme HB stars, EHB) in GCs have left many questions waiting for a proper answer (Moni Bidin & Piotto 2010).

The deep morphological differences observed among the HBs of the Galactic GCs are not fully explained because the cluster metallicity alone cannot account for them (Sandage & Wildey 1967; van den Bergh 1967). The HB morphology has been linked, among others, to cluster age (Dotter et al. 2010), cluster concentration (Fusi Pecci et al. 1993), stellar rotation (Peterson 1983), cluster mass (Recio-Blanco et al. 2006), and the environment of formation (Fraix-Burnet et al. 2009). However, none of the proposed second parameters could satisfactorily reproduce the complex observed behavior. Gratton et al. (2010) showed that a set of at least three parameters is required to describe the observations. The recent discovery that many clusters host stellar sub-populations with different helium content (Piotto et al. 2005, 2007) has given new strength to the proposition that helium abundance could be a key parameter governing the cluster HB morphology (D'Antona et al. 2002, 2005; Lee et al. 2005). In this scenario, the blue HB stars observed in many GCs would be the progeny of the He-enriched second stellar generation. Unfortunately, diffusion processes are active in the atmosphere of HB stars hotter than ∼11 500 K (Michaud et al. 1983, 2008; Quievy et al. 2009), causing photometric anomalies (Grundahl et al. 1999) and deep alteration of the surface

⋆ Based on observations with the ESO Very Large Telescope at Paranal Observatory, Chile (proposal ID 076.D-0810).

⋆⋆ Table 2 is available in electronic form at http://www.aanda.org, and also at the CDS via anonymous ftp to cdsarc.u-strasbg.fr (130.79.128.5) or via http://cdsarc.u-strasbg.fr/viz-bin/qcat?J/A+A/547/A109

chemical composition (Behr 2003). As a consequence, the direct measurement of the primordial helium abundance is possible only for blue HB stars cooler than about 11 500 K (Villanova et al. 2009, 2012). Moni Bidin et al. (2011a, hereafter Paper I) recently searched for indirect evidence of helium enrichment among blue HB stars in ω Centauri, a cluster known to host a very complex mix of at least six sub-populations (Bellini et al. 2010). Their results are surprisingly puzzling. In brief, the measured gravities are systematically lower than the predictions of canonical evolutionary models with solar helium abundance, in agreement with the expectations for He-enriched models. This behavior was not observed in three other clusters previously analyzed, and it is unique of ω Cen stars. However, the calculated masses are unrealistically low, and the low gravities can thus not be straightforwardly interpreted as a direct evidence of helium enrichment.

The UV color–magnitude diagram (CMD) of the most massive GCs has revealed an additional puzzling feature, the so-called blue hook (BH), a population of stars bluer than the canonical end of the HB (Whitney et al. 1998; Piotto et al. 1999; D'Cruz et al. 2000; Brown et al. 2001; Rosenberg et al. 2004; Momany et al. 2004; Busso et al. 2007; Ripepi et al. 2007). The formation of these extremely hot objects ($T_{\rm eff} \geq 32\,000$ K) cannot be explained by the canonical stellar evolution theories. They were proposed to be the progeny of stars that, due to an unusually large mass loss, left the red giant branch before the helium flash and ignited helium on the white dwarf cooling sequence (Castellani & Castellani 1993; D'Cruz et al. 1996; Brown et al. 2001). Due to the very low efficiency of the H-burning in the shell, and hence the very low entropy barrier present at the shell location, these stars can experience a He flash-induced mixing inside the He core able to reach the H-rich envelope (Sweigart 1997; Cassisi et al. 2003). As a consequence of this process, some amount of H can be dredged down the stellar interior, and He-burning products can be dredged up the stellar surface. Depending on the efficiency of this He flash-induced mixing, some hydrogen can remain in the envelope (Lanz et al. 2004), while the surface carbon abundance is increased to 1−5% by mass. On the other hand, Lee et al. (2005) suggested that BH stars in ω Cen are the progeny of the helium-enriched main sequence population. D'Antona et al. (2010) proposed that extra-mixing processes during the red giant phase can increase their surface helium abundance up to $Y \approx 0.8$, required to explain their photometric behavior. Their carbon abundance should, however, not be enhanced. The high carbon abundances found by Moehler et al. (2011) pose a problem to these scenarios, as they indicate that some extra process (beyond helium enrichment) is required to explain the BH stars. Moreover, while the majority of their targets above 30 000 K showed a solar or super-solar surface helium abundance, they detected a sub-population of very hot helium-poor EHB stars, which they propose are post-HB stars evolving toward the white dwarf cooling sequence.

We measured the surface parameters of a large sample of HB and BH stars in ω Cen to gather new information about their properties. The results for the temperature, gravities, and masses of the stars with $T_{\rm eff} \leq 32\,000$ K were presented in Paper I. In this paper, we will present the results on the surface helium abundance for all the stars, focusing on the BH candidates hotter than 32 000 K, which were not analyzed in Paper I. Whenever applicable, we will compare our results to those of Moni Bidin et al. (2007, 2009), who measured the parameters of HB stars in NGC 6752, M 80, and NGC 5986. At variance with ω Cen, these three clusters do not show main sequence (MS) splitting, although the MS of NGC 6752 is broadened (Milone et al. 2010). Moni Bidin et al. (2007, 2009) used the same instrument, software, and models as we did, and the comparison can thus easily reveal intrinsic differences between the clusters.

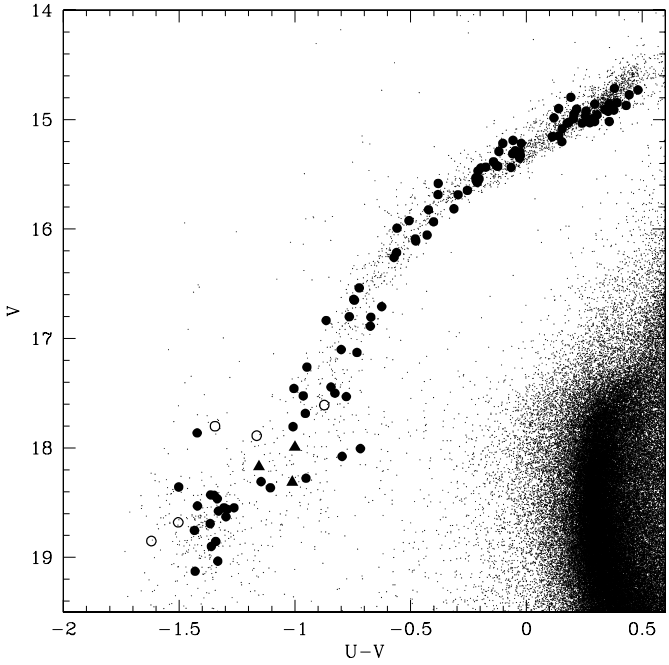

Fig. 1. Position of the target stars in the cluster CMD. The empty circles indicate hot ($T_{\rm eff} \geq 32\,000$ K) helium-poor stars. Full triangles show the objects with anomalously high spectroscopic mass.

2. Observations and data reduction

Our observations targeted 115 HB stars in ω Cen, selected from the optical photometry of Bellini et al. (2009). They span a wide range of the cluster HB, from the blue edge of the RR Lyrae gap ($T_{\rm eff} \sim 7800$ K) to BH candidates at $T_{\rm eff} \geq 32\,000$ K. The distribution of the targets in the cluster CMD is shown in Fig. 1.

The data were collected at the Paranal Observatory in service mode, with the FORS2 spectrograph mounted on the UT1 telescope. The observations were performed under a variety of sky conditions, as shown in the log of the observations given in Table 1. The instrument was used in multi-slit (MXU) mode, collecting between 12 and 24 spectra in each of the seven masks that were employed. The slit width of 0.″5 and the 600B grism returned a spectral resolution $R \approx 1600$ in the range 3450–5900 Å. Two 45-min exposures were acquired for the masks comprising only bright stars, while three similar exposures were collected when faint stars were involved. The final spectra thus had a signal-to-noise ratio between 40 and 180, although the targets span a range of about four magnitudes.

The spectra were de-biased, flat-fielded, and wavelength-calibrated with the FORS pipeline[1]. The accuracy of the wavelength calibration was ∼5 km s^{-1}. The spectra were then extracted with standard IRAF[2] routines. They were corrected subtracting the sky background within the same slit, whose

[1] http://www.eso.org/sci/data-processing/software/pipelines/index.html

[2] IRAF is distributed by the National Optical Astronomy Observatories, which are operated by the Association of Universities for Research in Astronomy, Inc., in cooperative agreement with the National Science Foundation.

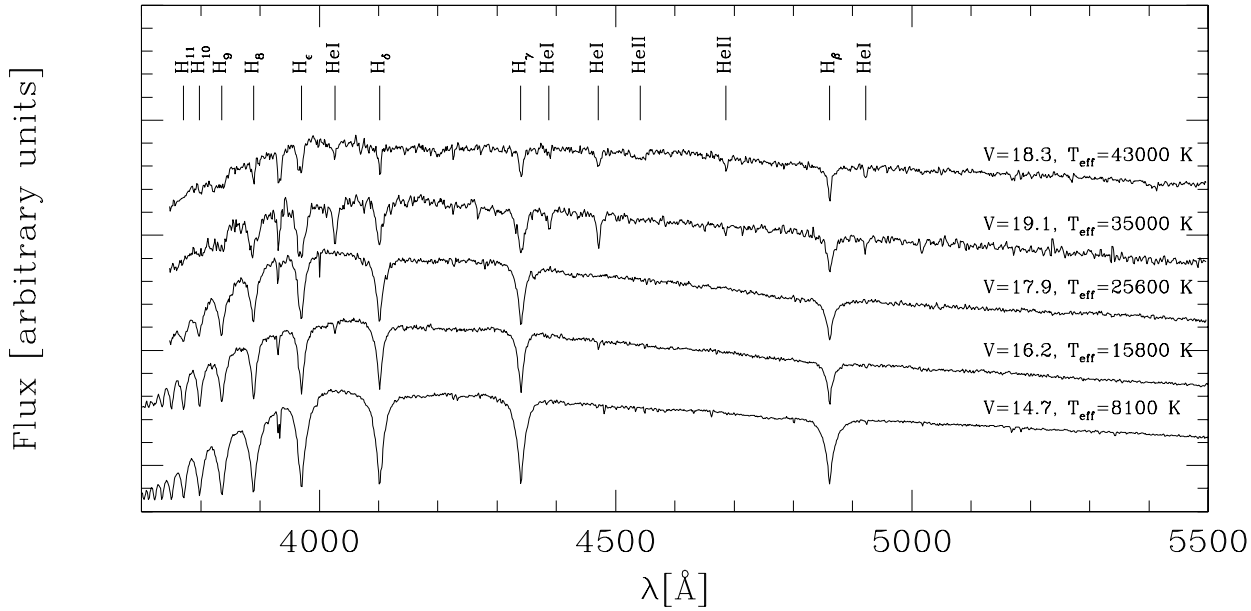

Fig. 2. Example of the flux-calibrated extracted spectra of stars at different temperatures. The hydrogen and helium lines used in the fitting routine are also indicated.

Table 1. Log of the observations.

Start of observation (UT)	Airmass	Seeing (″)	Moon distance (deg)	Moon illumination
2006-01-19T07:34:14	1.25	1.0	58	0.80
2006-01-19T08:02:00	1.19	0.9	57	0.80
2006-01-19T08:29:23	1.15	1.1	57	0.80
2006-02-09T07:42:57	1.11	0.7	120	0.86
2006-02-09T08:15:37	1.09	0.8	120	0.86
2006-02-09T08:49:06	1.09	0.7	119	0.86
2006-02-14T05:23:28	1.35	2.2	71	0.99
2006-03-23T08:47:02	1.30	0.6	63	0.43
2006-03-23T09:00:09	1.34	0.5	63	0.43
2006-03-31T07:54:08	1.27	1.5	148	0.05
2006-04-01T06:24:15	1.12	0.8	147	0.11
2006-04-01T06:55:04	1.15	0.7	147	0.11

minimum length was 6″, and then flux-calibrated. The response curve was obtained from the spectrum of the standard star LTT4816 (Hamuy et al. 1992), collected during the observations. Some examples of the reduced spectra are shown in Fig. 2.

The heliocentric radial velocity (RV) of the target stars was measured with the IRAF task *fxcor*. Each spectrum was cross-correlated (Tonry & Davis 1979) with a synthetic template with temperature and gravity similar to those of the target, as deduced from its position on the cluster HB. Previous investigations have shown that the RV measurements are negligibly affected by the exact choice of the template (Morse et al. 1991; Moni Bidin et al. 2011b). The results are given in the tenth column of Table 2, and the distribution of the RVs is shown in Fig. 3. The error deriving from the cross-correlation procedure is ∼30 km s^{-1}. The mean RV of the sample is $\overline{\mathrm{RV}}$ = 231.9 ± 3.4 km s^{-1}, in excellent agreement with the cluster RV of 232.1 km s^{-1} quoted by Harris (1996, 2010 December Web version[3]). The velocities follow a Gaussian distribution with no evident outliers, and they are therefore compatible with the assumption that all the targets are cluster members. However, the observed dispersion is 37.1 ± 2.4 km s^{-1}, larger than that expected from the observational errors and the internal cluster dispersion (∼13 km s^{-1}, Sollima et al. 2005). In fact, quadratically subtracting the estimated wavelength calibration and measurement errors, we obtain an intrinsic dispersion of ∼21 km s^{-1}, incompatible with the cluster internal dispersion at any distance from the center (Scarpa & Falomo 2010). This most probably indicates that the imperfect centering of the targets inside the slits introduced an additional error of the order of ∼20 km s^{-1}, i.e., about one tenth of resolution element, or 0.4 pixels. This effect is frequent in multi-object slit spectroscopy (see the analysis of Moni Bidin et al. 2006).

3. Measurements

The temperature, gravity, and atmospheric helium abundance of the target stars were measured by fitting the observed hydrogen and helium lines with synthetic spectra. The stars at the coolest end of our sample ($T_{\rm eff} \leq 12\,000$–$13\,000$ K) were fitted with a grid of model spectra computed with Lemke's version[4] of the LINFOR program (developed originally by Holweger, Steffen, and Steenbock at Kiel University), fed with local thermodynamic equilibrium (LTE) model atmospheres of cluster metallicity ([M/H] = −1.5) computed with ATLAS9 (Kurucz 1993). The helium abundance was kept fixed to solar value, as expected for stars not affected by diffusion processes, because the He lines of cool stars are weak and not observed at our resolution. Stars hotter than 13 000 K, as deduced from their position in the CMD, or showing evidence of active atmospheric diffusion, i.e., strong iron lines between 4450 and 4600 Å (Moehler et al. 1999), were fitted with models of super-solar metallicity ([M/H] = +0.5) and variable surface helium abundance to account for the effects of radiative levitation of heavy elements (Moehler et al. 2000). This was done even for five warm stars not fully satisfying these criteria (stars #82876, #133061, #75469, #100288,

[3] http://physwww.physics.mcmaster.ca/%7Eharris/mwgc.dat

[4] http://a400.sternwarte.uni-erlangen.de/~ai26/linfit/linfor.html

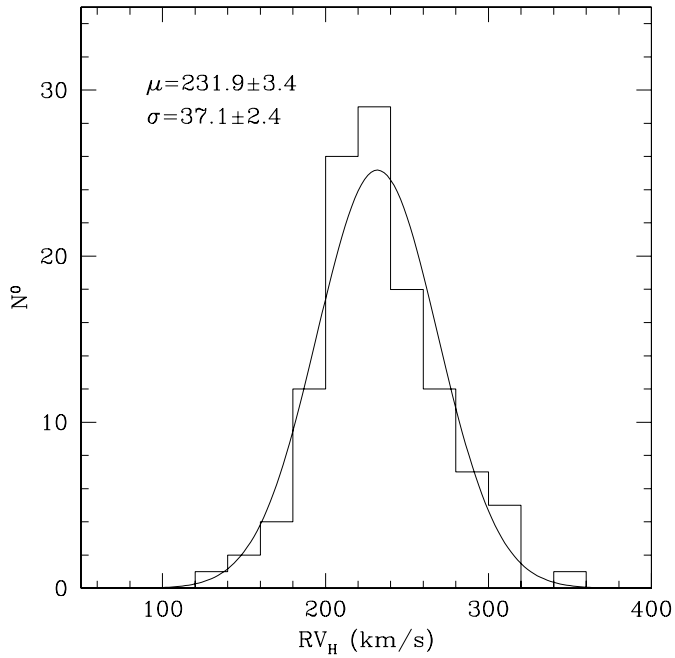

Fig. 3. Histogram of the distribution of the measured heliocentric RVs. A Gaussian fit with the given mean and dispersion is also indicated.

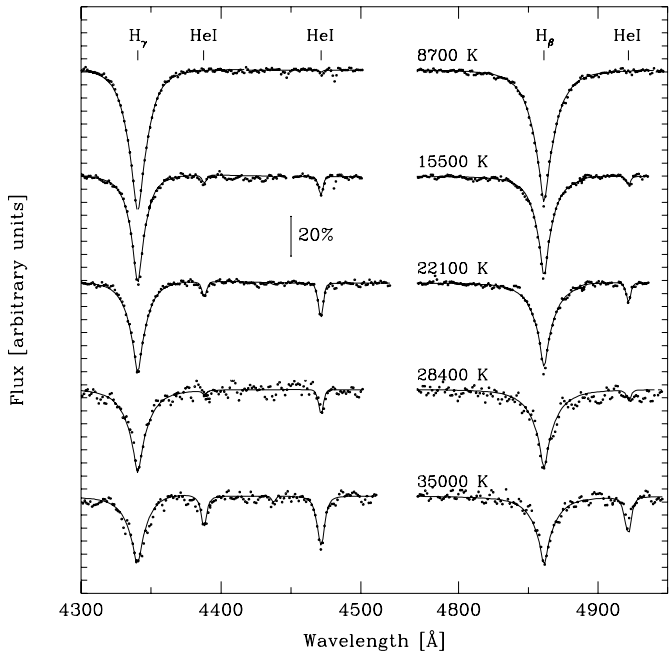

Fig. 4. Example of fit of the most prominent spectral features. The observed spectra are shown with circles, the best-fit synthetic spectrum is indicated by the full curve.

and #100817, with $T_{\rm eff}$ = 11 500−13 000 K), because the helium lines of the model with solar helium abundance were too strong compared to the observed ones. The helium abundance was thus determined during the fitting routine. Stars bluer than the canonical end of the EHB in the CMD ($T_{\rm eff} \geq 32\,000$ K) were fitted with the grid of metal-free non-LTE models described in Moehler et al. (2004), calculated as in Napiwotzki (1997). We found that the use of these models did not improve the quality of the fit (expressed by the χ^2 statistics) for stars between 30 000 and 32 000 K. When the routine indicated a helium abundance next to solar ($\log(N_{\rm He}/N_{\rm tot}) = -1$) or higher, the fit was repeated with the helium-rich non-LTE models, calculated with a modified version of the code of Werner & Dreizler (1999), with the model atoms of Werner (1996). The star #178139 was fitted with helium-poor models, despite its solar helium abundance, because the use of the He-rich models degraded the quality of the fit noticeably.

The routines developed by Bergeron et al. (1992) and Saffer et al. (1994), as modified by Napiwotzki et al. (1999), were used to derive the stellar parameters. They normalize both the model and observed spectra using the same points for the continuum definition and employ a χ^2 test to establish the best fit. The noise in the continuum spectral regions is used to estimate the σ for the calculation of the χ^2 statistics, which the routines use to estimate the errors on the parameters (see Moehler et al. 1999). However, they thus neglect other sources of errors, such as those introduced by the normalization procedure, the sky subtraction, and the flat-fielding. Therefore, the resulting uncertainties were multiplied by three to obtain a more realistic estimate of the true errors (Napiwotzki 2005, priv. comm.). The lines used in the fitting procedure included the Balmer series from H_β to H_{12}, except the H_ϵ to avoid the blended Ca II H line, and four He I lines (4026 Å, 4388 Å, 4471 Å, 4922 Å) for the stars whose helium abundance was a free fit-parameter. Two He II lines (4542 Å, 4686 Å) were also used, when visible, in the spectra of the hottest stars. Some fits of the observed spectral features are shown in Fig. 4 as an example for two Balmer and three He I lines of five stars at different temperatures.

Stellar masses were estimated from the derived stellar parameters through the relation

$$\log\frac{M}{M_\odot} = \log\frac{g}{g_\odot} - 4\cdot\log\frac{T_{\rm eff}}{T_{\rm eff,\odot}} + \log\frac{L}{L_\odot}, \quad (1)$$

where

$$\log\frac{L}{L_\odot} = -0.4\cdot(V-(m-M)_0-3.1\cdot E(B-V)+BC_V-M_{\rm bol,\odot}). \quad (2)$$

We assumed $T_\odot$ = 5777 K, $\log g_\odot$ = 4.44, $(m-M)_0$ = 13.75 ± 0.13 (van de Ven et al. 2006), and $E(B-V)$ = 0.12 ± 0.01 (Harris 1996, December 2010 Web version). We adopted this reddening for all the stars instead of the value spectroscopically derived for each target (Sect. 4.2), because our results are scattered around this mean reddening, with negligible trend with temperature. Hence, the use of the individual reddening only adds noise without altering the general trend. The bolometric correction (BC_V) was derived from the effective temperature through the empirical calibration of Flower (1996). We therefore fixed $M_{\rm bol,\odot}$ = 4.75 because $M_{V,\odot}$ = 4.83 (Binney & Merrifield 1998), and the Flower (1996) $BC_V - T_{\rm eff}$ relation returns $BC_\odot = -0.08$. Errors on masses were derived from propagation of errors. The resulting temperature, gravity, helium abundance, and mass of each target are given in Table 2.

4. Results

4.1. Comparison with Moehler et al. (2011)

Our sample comprises 11 stars studied by Moehler et al. (2011). They are indicated with an "M" in the last column of Table 2. Moehler et al. measured the stellar parameters with the same procedure and software used by us, but with high-resolution spectra of shorter wavelength coverage. They also employed the

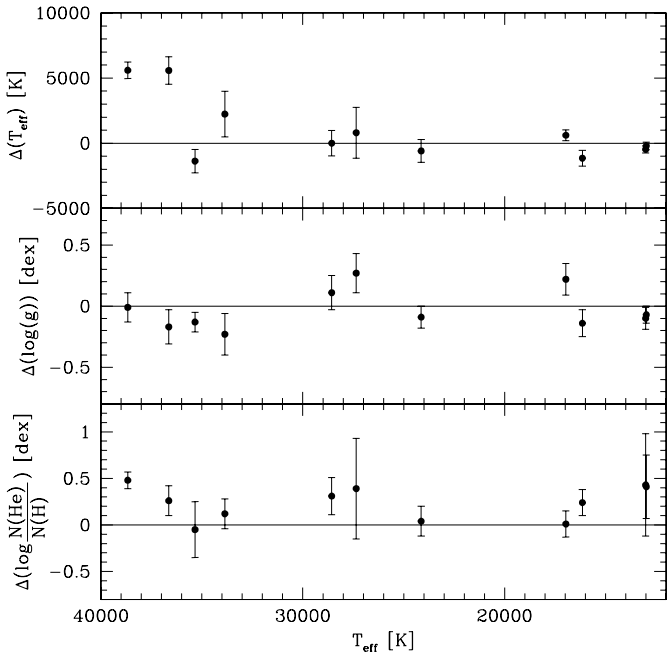

Fig. 5. Comparison between our results and those of Moehler et al. (2011) for the 11 stars in common. The differences (in the sense ours − Moehler et al.'s) in temperature (*upper panel*), gravity (*central panel*), and helium abundance (*lower panel*) as a function of temperature are shown.

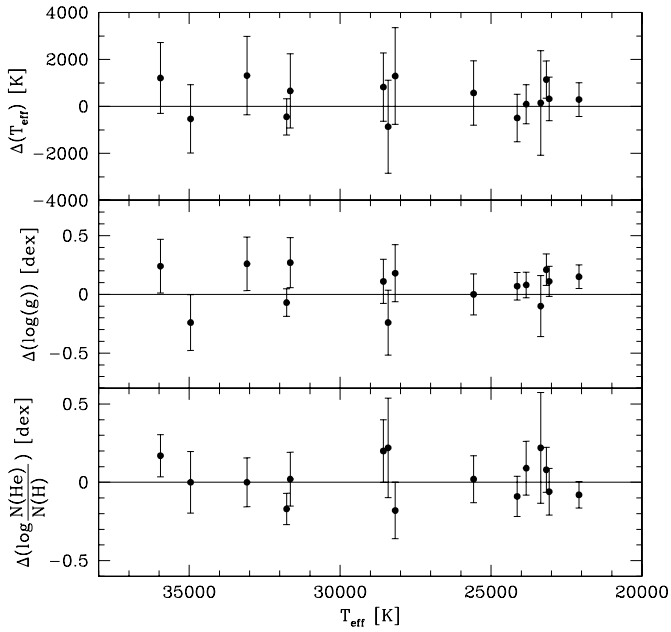

Fig. 6. Same as Fig. 5, but comparing our results with those derived by analysing our data using the model spectra of Moehler et al. (2011).

same models for stars with $T_{\rm eff} \leq 20\,000$ K, while for hotter stars they used metal-poor ([M/H] = −1.5) non-LTE model atmospheres. The comparison for the stars in common is shown in Fig. 5, where the error bars indicate the quadratic sum of the uncertainties in the two works. As commented in Paper I, the temperature and gravity measured in the two investigations for the seven stars in common cooler than 32 000 K agree well: the mean differences (ours − Moehler et al.'s) are only $\Delta(T_{\rm eff}) = -143$ K and $\Delta(\log g) = 0.03$ dex. Our mass estimates are on average higher by 0.08 $M_{\odot}$, as a consequence of the fainter magnitudes of the Castellani et al. (2007) catalog, adopted by Moehler et al. (2011). On the contrary, the four hottest stars suggest that some systematic could be present between the BH stars. In fact, our temperatures are on average higher by ∼3000 K, and our gravities (and masses) lower by ∼0.14 dex. The use of different models is expected to cause such effect (Dreizler 2012, priv. comm.), but the stars in common are too few and the detected offsets could not be significative. For example, the difference in temperature is entirely due to the two hottest stars only.

To investigate further the systematics introduced by the use of different models, we re-fitted a subset of 15 stars with $T_{\rm eff} \geq 20\,000$ K (indicated with "T" in the last column of Table 2) with the same models used by Moehler et al. (2011), calculated with TLUSTY[5] (Hubeny & Lanz 1995). More details about the model atoms and the atomic data can be found in Lanz & Hubeny (2003, 2007) and Moehler et al. (2011). The comparison between the parameters obtained with our models and these non-LTE ones (in the sense our models − TLUSTY) is shown in Fig. 6, where the error bars indicate the quadratic sum of the errors in the two measurements. The comparison only partially explains the differences with Moehler et al. (2011) results. The temperatures measured with our models are higher, but by only ∼370 K on average, much less than the differences seen at the hotter end of Fig. 5. Our gravities are higher, and not lower, by 0.07 dex, which is not a significative offset compared to the errors. In both cases, no trend with temperature is observed. We also note that the differences in temperature and gravity are strongly correlated. As an additional test, we repeated the measurements on the Moehler et al. (2011) FLAMES spectra, after degrading their resolution to match that of FORS data. Very similar results were found, with no evidence of a significant offset in temperature or gravity. In conclusion, the use of different models accounts only for a small offset in temperature. The differences with Moehler et al.'s results could be an effect of the small quantity of hot stars in common. However, other evidences later in our analysis (Sects. 4.4 and 4.6) suggest that an offset could indeed be present.

Figure 5 shows an offset in the surface helium abundances, our measurements being systematically higher than those of Moehler et al. (2011) by 0.24 dex on average. No trend with temperature is visible. This offset is not due to the use of different models, as evidenced by the lower panel of Fig. 6, where no systematic is found. Moreover, the difference is present at any temperature, even for stars cooler than 20 000 K, where the same models were used in both works. Moehler et al. (2011) used three of our four He I lines, and we verified that repeating our measurements with their line list only caused random changes on the derived helium abundance, with an rms of ∼0.03 dex. This is therefore not the cause of the observed systematic, which should be related to the different resolution. Very interestingly, Moni Bidin et al. (2009) suggested that their helium abundances could be systematically higher, by a quantity similar to what was found here, compared to the collection of literature measurements of field stars presented by O'Toole (2008), which is based on spectra of higher resolution (Edelmann et al. 2003; Lisker et al. 2005; Ströer et al. 2005; Hirsch et al. 2008). Moni Bidin et al. (2009) used the same instrument and resolution as in the present work. There should therefore be a systematic difference between measurements based on data with different resolution, with the lower resolution returning higher helium abundances

[5] http://nova.astro.umd.edu

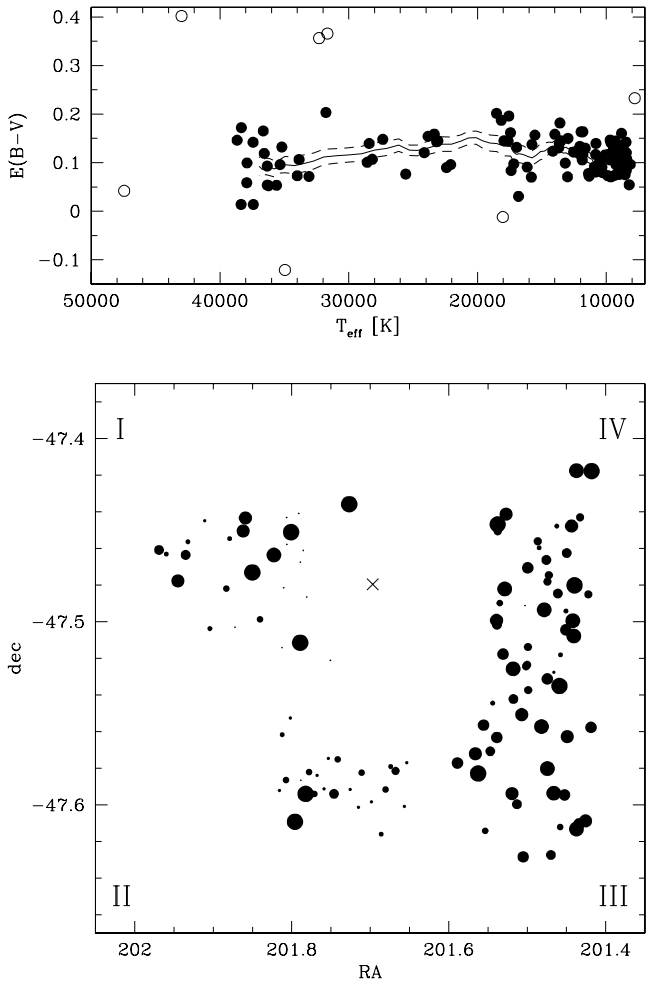

Fig. 7. *Upper panel*: reddening estimates for program stars as a function of temperature. The deviant points are indicated with empty circles. The trend of the mean reddening (calculated as described in the text) with its 1-σ stripe is shown with full and dashed lines, respectively. *Lower panel*: spatial distribution of the observed stars, where the size of each plotted point is proportional to the star's reddening. The cross indicates the cluster center.

by about 0.2−0.25 dex. More detailed investigations would be needed to further analyze this behavior.

4.2. Reddening

We estimated the reddening of each target, comparing the observed $(B-V)$ color from the Bellini et al. (2009) catalog with the theoretical color of a star with the same temperature and gravity. This value was determined interpolating the Kurucz (1993) grid of models with the same metallicity used in the spectra fitting procedure. The results are shown in the upper panel of Fig. 7, where seven stars deviating from the general trend are evidenced. The surface parameters of these stars are not peculiar, but we notice that half of them have very low spectroscopic mass (0.2−0.3 $M_{\odot}$, see Fig. 13) and the three targets with $E(B-V) \geq 0.3$ are all redder than the mean HB in Fig. 1 ($V \geq 18$, $U-V \geq -1$). After their exclusion, the mean reddening is $E(B-V) = 0.115 \pm 0.004$, and the stars are scattered about this value with an rms of 0.037 mag. These values excellently agree with previous investigations, which found $E(B-V) = 0.11$−0.12 (Lub 2002; Bedin et al. 2004; Calamida et al. 2005; Cassisi et al. 2009). In Fig. 7, we also show the trend of the mean reddening, which was calculated by substituting to each target the mean value of the ten adjacent stars in temperature order. The 1-σ stripe was calculated from the statistical error-on-the-mean of this estimate. Moreover, $E(B-V)$ shows only a tiny trend with temperature, which is not significative within errors. The reddening effect is expected to increase for bluer spectral types (Grebel & Roberts 1995), and in fact the mean value increases from 0.110 ± 0.005 for stars between 8000 and 10 000 K to 0.123 ± 0.008 in the range 20 000−30 000 K. Among stars hotter than 32 000 K, we find a mean reddening that is slightly lower (0.098 ± 0.012), but still consistent within errors with the cooler stars. In any case, the temperature offset discussed in Sect. 4.1 cannot be related to this, because a temperature overestimate would cause a higher reddening. The great majority of these stars are helium rich (86%, see Sect. 4.4), and it could be argued that the derived lower reddening is due to this discontinuity in the surface chemical composition. However, we found no evidence that $E(B-V)$ is on average higher for the three helium-poor objects in this temperature regime. On the other hand, it must be taken into account that the theoretical $(B-V)$ color has been obtained from a grid of LTE models that should be inadequate for hotter stars. This could have caused the small offset observed for these targets.

In conclusion, the measured reddening agrees with the literature, confirming that the spectroscopic temperatures are good. For example, a temperature scale hotter by 10% would have caused an overestimate of reddening by 0.04 mag at 10 000 K. We therefore do not find the problems that Moni Bidin et al. (2007) presented in NGC 6752. Hence, we exclude the theoretical colors of the ATLAS9 grid as the origin of their reddening underestimate.

The derived reddening estimates can be used to analyze the pattern of $E(B-V)$ in the cluster area. The position of the target stars, with symbols proportional to the measured reddening, is shown in the lower panel of Fig. 7. The resulting map is far from uniform, because the stars in the eastern side of the cluster are on average less reddened than in the western half. The average value of $E(B-V)$ is 0.127 ± 0.05 and 0.133 ± 0.04 in the fourth and third quadrant, respectively, while it is 0.11 ± 0.02 in the first and 0.097 ± 0.008 in the second one. The reddening is therefore uniform in the western half of the cluster, within the limits of our accuracy. On the eastern side, on the contrary, the reddening is lower, in particular, in the southeast quadrant. This observed pattern is not a consequence of an uneven distribution of the hotter stars, whose measured reddening is slightly lower than the average (see the upper panel of Fig. 7, and discussion above in this section). In fact, we have an equal number of BH candidates in both the eastern and western half, and none in the second quadrant, where the average reddening is the lowest. A more detailed map of the cluster differential reddening is prevented by the limited number of data points and by the non-uniform area sampling. Despite our limitations, our results match the pattern found by Calamida et al. (2005), who found the clumpy structure of reddening in the direction of ω Cen, with more reddened stars clustering on the west side, and in particular in the northwest quadrant.

4.3. Helium abundance: canonical blue HB stars ($T_{eff} \leq 32\,000$ K)

The surface helium abundance of target stars cooler than 32 000 K is plotted in the upper panel of Fig. 8 as a function of the effective temperature. The results of Moni Bidin et al. (2007) and Moni Bidin et al. (2009) in NGC 6752, M 80, and

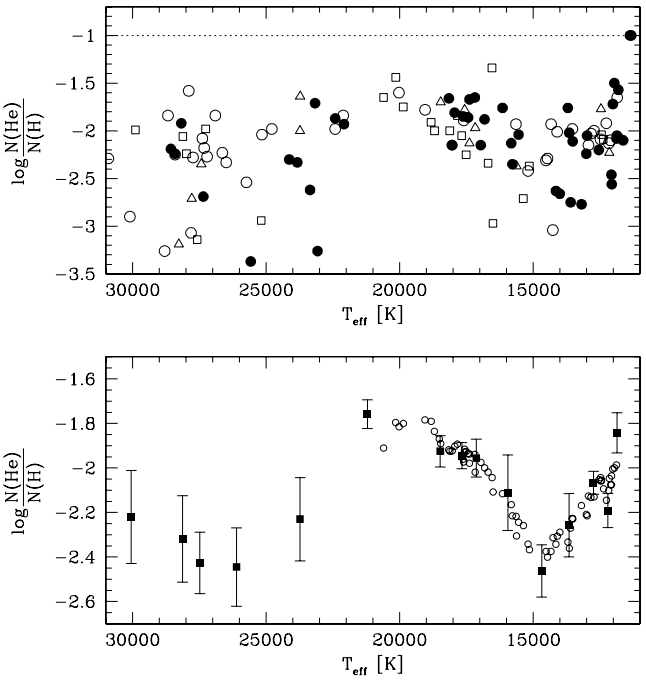

Fig. 8. *Upper panel*: surface helium abundance of cooler stars as a function of temperature. The dotted line indicates the solar value ($Y = 0.25$). Filled circles: this work; empty circles: NGC 6752 (Moni Bidin et al. 2007); empty triangles and squares: NGC 5986 and M 80, respectively (Moni Bidin et al. 2009). *Lower panel*: trend of surface helium with temperature, obtained binning the data of the upper panel with two different binning schemes (see text for details).

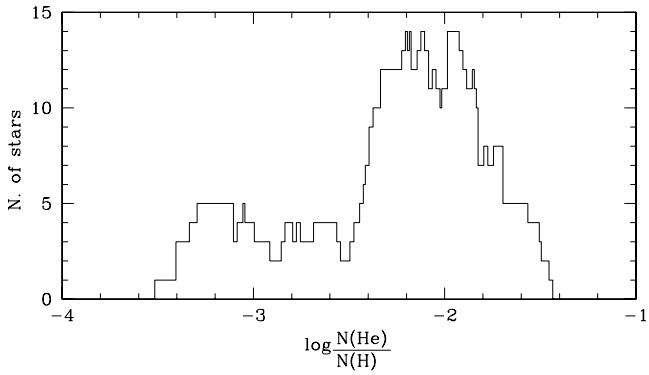

Fig. 9. Histogram of the distribution of the surface helium abundance of EHB stars ($T_{\rm eff} \geq 20\,000$ K) in ω Cen, NGC 6752 (Moni Bidin et al. 2007), NGC 5986, and M 80 (Moni Bidin et al. 2009).

NGC 5986 are also plotted, while we exclude the measurement of Moehler et al. (2011) from the comparison, because of the offset discussed in Sect. 4.1. HB stars in ω Cen follow the same trend as their counterparts in the other clusters, despite the peculiarities described in Paper I. As well known, the atmospheric diffusion erases the chemical differences between stars in clusters of different metallicity (Behr 2003; Pace et al. 2006).

The surface helium abundance of the targets between 11 500 and 20 000 K follows the trend discovered by Moni Bidin et al. (2009). This is seen clearly in the lower panel of Fig. 8, where the measurements in all the clusters are averaged following two binning schemes. In the first scheme, shown with full squares, the targets are binned in non-overlapping groups of 15 stars each. The error bars indicate the statistical error-on-the-mean in each bin. The empty circles, on the contrary, show the result of substituting each data point with the average of the ten adjacent points, in order of temperature. As known for many decades (Baschek 1975; Heber 1987; Glaspey et al. 1989), the atmosphere of HB stars hotter than 11 500 K is depleted in helium because it settles toward deeper layers as an effect of diffusion (Greenstein 1967). The observed change is, however, not abrupt, because the surface He abundance smoothly decreases with temperature up to $T_{\rm eff} \approx 15\,000$ K, where it reaches a minimum. Beyond this temperature, the helium abundance reverts its trend, slowly increasing again up to ≈20 000 K. This behavior can be observed even in Moehler et al. (2003, see their Fig. 5) and partially in Behr (2003) and Fabbian et al. (2005). A similar turnoff of the surface iron abundance at ≈15 000 K can be observed in Pace et al. (2006). Hence, the trend is not a systematic error, but it indicates that the efficiency of the atmospheric diffusion varies with temperature along the HB, as discussed in detail by Moni Bidin et al. (2009).

The results for stars hotter than 20 000 K are scattered in a wide range of nearly two orders of magnitudes, much larger than the observational errors (0.1−0.2 dex at these temperatures). The binned data (lower panel of Fig. 8) suggest a mild increase of the mean abundance for $T_{\rm eff} \geq 27\,000$ K. This trend is not significant compared to the dispersion of the points, as indicated by the large error bars associated to the average values, but it coincides with what has been observed among field stars (see Fig. 1 of O'Toole 2008). Edelmann et al. (2003) discovered a family of extremely helium-poor field EHB stars, comprising ∼10% of the whole population, with a surface helium abundance 1−1.5 dex lower than the other EHBs. Thus, a bimodal distribution of $\log(N({\rm He})/N({\rm H}))$ should be expected, even in GCs. The histogram shown in Fig. 9 suggests that this could be the case. It was obtained associating to each value of $\log(N({\rm He})/N({\rm H}))$ the quantity of stars with helium abundance within ±0.15 dex, which is the mean observational error at these temperatures. The distribution is relatively smooth, but at least two main peaks are visible, at about $\log(N({\rm He})/N({\rm H})) = -2$ and −3.2 dex, A gap, or even a third peak, could be present at about −2.8 dex. Two out of the fourteen EHB stars in ω Cen have $\log(N({\rm He})/N({\rm H})) \leq -2.8$, corresponding to 14%, compared to 15% found in NGC 6752. These objects are apparently more frequent in M 80 and NGC 5986 (22% and 40%, respectively), but the statistics is not significative due to the small observed samples. In conclusion, about 15% of the EHB stars in the four GCs have very low surface helium abundance. However, they are not clearly separated from the other more numerous EHB objects, and the evidence for a bimodal distribution is not conclusive. The position of the two extremely He-poor EHB stars in ω Cen in the CMD and in the temperature-gravity plane is not distinct from the distribution of the other stars, as shown in Figs. 1 and 11.

4.4. Helium abundance: blue hook candidates

The surface helium abundance of our hottest targets is shown in Fig. 10. Two distinct groups of stars are clearly visible: the atmosphere of few stars with $\log(N({\rm He})/N({\rm H})) \leq -2.2$ is depleted in helium by more than one dex with respect to the majority of the stars, which exhibit a solar or super-solar abundance ($\log(N({\rm He})/N({\rm H})) \geq -1.1$). While Moehler et al. (2011) found that 28% of their stars in the range 30 000−50 000 K is He-poor, we detect a lower fraction (14%). This difference could partially be an effect of a small number statistics, but it is moderately significative because, given the statistics of

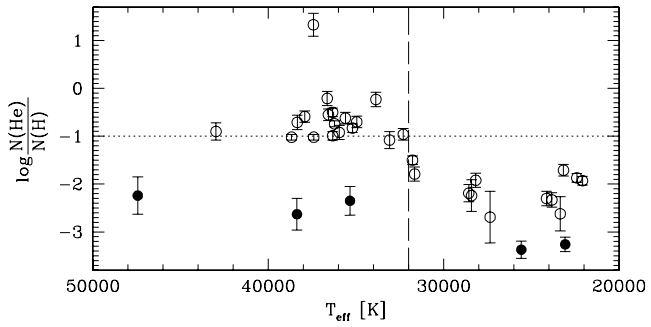

Fig. 10. Surface helium abundance of the hottest targets as a function of temperature. The helium-depleted stars discussed in the text are indicated with filled circles, while all the other stars are shown with empty circles. The dashed line at $T_{\rm eff}$ = 32 000 K separates the EHB stars from the BH candidates, while the dotted line indicates the solar helium abundance (Y = 0.25).

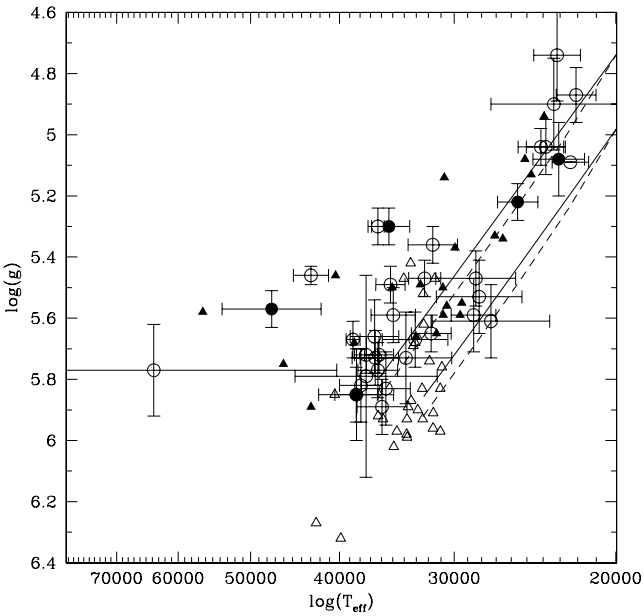

Fig. 11. Position of the hottest targets in the temperature-gravity plane. Big circles: this work; small triangles: data from Moehler et al. (2011). Empty and full symbols refer to the helium abundances of the objects as defined in the text and shown in Fig. 10. The full and dashed lines show the position of the canonical zero-age and terminal-age HB for canonical and helium-enriched stars, respectively.

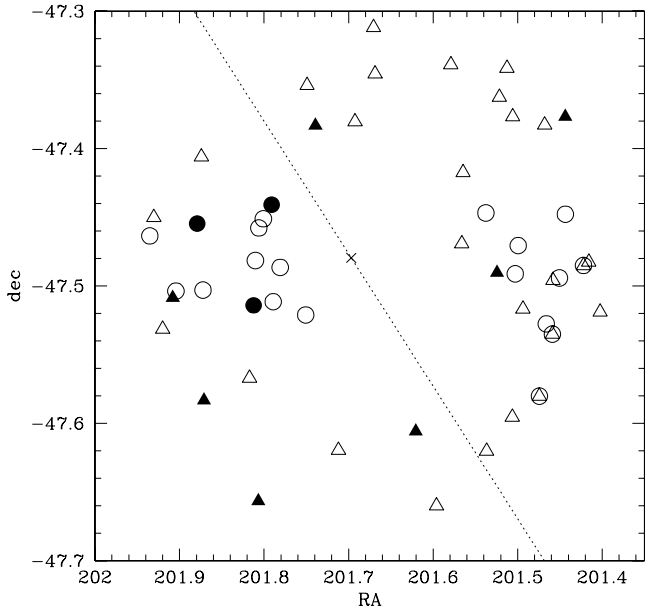

Fig. 12. Spatial distribution of the BH stars. The symbols are as in Fig. 11. The cross shows the position of the cluster center, while the dotted line cuts the cluster area as defined in the text.

Moehler et al. (2011), our results have a probability of 10% of being due to pure chance. Moreover, we notice that Moehler et al. (2011) measured even a fraction of extremely He-poor EHB stars ($\log(N(\mathrm{He})/N(\mathrm{H})) \leq -3$, $T_{\rm eff}$ = 20 000–32 000 K) a factor of two higher (~40%) than in the present work. The discrepancy could be reduced if, strictly adopting the temperature range used by Moehler et al. (2011) and taking into account the offset of ~0.2 dex in He abundance between the two works discussed in Sect. 4.1, we considered the two stars at ~31 000 K and $\log(N(\mathrm{He})/N(\mathrm{H})) \approx -1.7$ as He-depleted BH objects. However, comparing Fig. 10 with the trend of field stars (Fig. 1 of O'Toole 2008), these targets appear most likely as the connection between the EHB and BH sequences richer in helium. This kind of transitional objects is missing in the Moehler et al. (2011) sample.

Moehler et al. (2011) showed that the helium-poor hot stars in their sample are most likely evolving off the HB. In fact, the evolutionary path of post-EHB stars, after the exhaustion of helium in the core, draws the stars toward lower gravities and higher temperatures (see, for example, Moehler et al. 2004), while they become bluer and brighter. The position of two of our helium-poor very hot targets in the CMD and in the temperature-gravity plane, shown in Figs. 1 and 11 respectively, differs from the bulk of BH objects, indicating that they also are most probably evolving toward the white dwarf cooling sequence. A third helium-depleted object (#181428) is, on the contrary, not distinct to the helium-rich stars, and its nature is more uncertain. As already discussed in Sect. 4.1, Fig. 11 suggests that an offset between our measurements and those of Moehler et al. (2011) at the hottest end of the distribution could be present, because their helium-rich targets at $\log g \geq 5.8$ cluster on the theoretical zero-age HB (ZAHB), while ours do not.

4.5. Spatial distribution of BH stars

Moehler et al. (2011) found an asymmetric spatial distribution for their helium-rich BH stars, which are more concentrated in the northwestern part of the cluster. Their helium-depleted targets, on the contrary, do not show such asymmetry. The spatial distribution of our targets and those from Moehler et al. (2011) are shown in Fig. 12. In both cases, however, the cluster is not uniformly sampled, and this introduces selection effects that must be taken into account. In fact, Moehler et al. (2011) also found that the helium-rich stars in the northwestern half of the cluster outnumber those in the other half by a factor of 2.7, but in that area they observed twice the quantity of targets than in southeastern half. However, the relative quantity of helium-poor to helium-rich stars should not be affected by any bias, because the photometric selection criteria are uniform in the whole cluster area. The helium-poor stars found by Moehler et al. (2011) are more frequent in the southeast side of the cluster (42%) with respect to the other half (14%).

Our sample consists of two distinct groups of stars of approximatively the same quantity of stars, one east and the other west of the cluster center. As the helium-rich stars dominate the

sample (Sect. 4.4), it is no surprise that we find a similar quantity on both sides of the center (nine stars, both in the east and west group), and no asymmetry is detected. However, the three helium-poor objects are found on the east side only. Dividing the cluster along a line with position angle 35° counted from north toward east, we thus detect a high fraction of helium-poor stars in the southeast half (25%), while no such object is detected out of nine stars in the other half. Hence, if we analyze their frequency instead of their absolute quantity, our results confirm those of Moehler et al. (2011). Merging the two samples and taking into account that four targets are in common, the resulting fractions are 11% (three out of 28 stars) and 30% (seven out of 23), in the northwest and southeast half, respectively. However, the evidence for an asymmetric distribution of the helium-poor targets is only mildly significative: a two-dimensional Kolmogorov-Smirnov test, performed following the recipes of Peacock (1983), reveals that there is a ∼11% probability that they are randomly drawn from the distribution of the observed sample. We conclude that the present observations suggest that an intriguing asymmetry could be present, but the result is not conclusive. A more systematic investigation, uniformly sampling the cluster area with a larger sample, would be required to clarify the issue. As already noted by Moehler et al. (2011), the suspected asymmetry is similar to the pattern of differential reddening evidenced by Calamida et al. (2005), discussed in Sect. 4.2, with helium-poor stars being more frequent in the less reddened part of the cluster. This connection is not straightforwardly explained. A selection effect could be introduced by the photometric target selection, if helium-poor stars are on average bluer than the helium-rich objects, but still the differential reddening that we find ($\Delta E(B-V) \approx 0.03-0.04$) is not large enough to hide blue objects in the more reddened regions.

4.6. Masses

In Paper I, we discussed the problem of the strong underestimate of the masses calculated for the stars cooler than 32 000 K. Analogous results were also obtained by Moehler et al. (2011), and the interpretation of this systematic was not straightforward. In Fig. 13 we show the results for the hotter end of our sample. Our mass estimates are too low even for the hot targets, contrary to Moehler et al. (2011), whose measurements agreed with the model expectations. Our underestimate could be easily explained by the offset in temperature and/or surface gravity for our hottest stars, discussed in Sect. 4.1 and suggested by Fig. 11. According to Eq. (1), either a temperature overestimate by ∼3000 K or a gravity underestimate by ∼0.14 dex causes an underestimate of the mass by about 35%. Correcting an offset of this magnitude would increase the average mass of these stars from ∼0.37 to ∼0.5 $M_\odot$, in agreement with Moehler et al. (2011) and with the theoretical expectations. However, the contemporary presence of both systematics, as suggested by Fig. 5, would result in a mass overestimate for the hottest targets of ∼0.23 $M_\odot$ on average.

Moni Bidin et al. (2007) discovered eight EHB stars in NGC 6752 with anomalously high spectroscopic mass, which possibly occupy redder and fainter loci in the CMD. Identical results were also found in M 80 (Moni Bidin et al. 2009). In ω Cen, we detect three EHB stars out of 14 (21%) with spectroscopic mass more than 0.1 $M_\odot$ higher than the other targets at the same temperature. All these objects have a surface helium abundance higher than $\log(N(\mathrm{He})/N(\mathrm{H})) = -2.7$, and none belongs to the extremely helium-poor sub-population. Their position in the cluster CMD is shown as filled triangles in Fig. 1. They are, indeed, on average, fainter and/or redder than the other main HB population. We detect a lower fraction of anomalous stars with respect to NGC 6752 and M 80, where they constituted the ∼40% of the analyzed sample in both cases. However, this difference is not very significative, because the probability of detecting only three anomalous stars in our sample, assuming that they are the 40% of the population, is 12%.

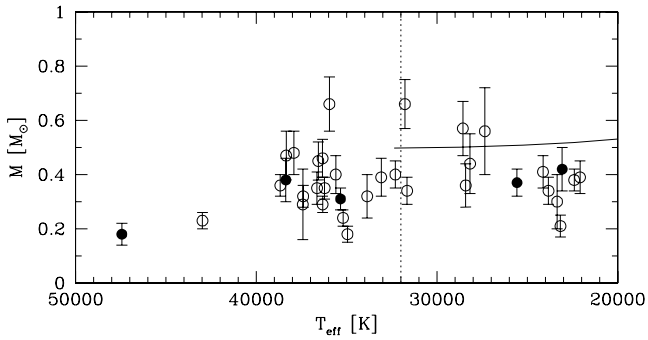

Fig. 13. Spectroscopic masses of the hottest targets as a function of temperature. The full line shows the canonical model expectations. Empty and full symbols are used for helium-rich and helium-poor stars, respectively, as defined in the text and shown in Fig. 10 with the same symbols.

4.7. Color–temperature relation

In Fig. 14, the spectroscopic temperature of the target stars is plotted against their observed color. This was dereddened assuming $E(B-V) = 0.115$, as measured in Sect. 4.2, and $E(U-V) = 0.194$ from the Cardelli et al. (1989) transformations of reddening in different bands. After the exclusion of some deviating stars, the fit of the data points in Fig. 14 returns the analytical expressions

$$\log(T_{\rm eff}) = 3.9646 - 0.1920 \cdot (U-V) + 0.1265 \cdot (U-V)^2, \quad (3)$$

$$\log(T_{\rm eff}) = 3.9438 - 0.7769 \cdot (B-V) + 5.6725 \cdot (B-V)^2. \quad (4)$$

The rms of the residuals in $\log(T_{\rm eff})$ is 0.035 dex for Eq. (3), and 0.070 for Eq. (4). The $(B-V)$ color is, as expected, much less sensitive to temperature than $(U-V)$, as indicated by the steeper solution.

In Fig. 14, the theoretical ZAHB from Pietrinferni et al. (2006) and Cassisi et al. (2009) with $Z = 0.001$ and $Y = 0.246$ for the α-enhanced mixture is overplotted to the data as a grey solid curve. Fifty-one HB stars of NGC 6752 are also plotted, whose spectroscopic temperatures and colors are taken from Moni Bidin et al. (2007) and Momany et al. (2002), respectively. Moni Bidin et al. (2007) measured a too low reddening for these stars, arguing that the photometric data could suffer from a zero-point offset. Following their results, $(B-V)$ was not corrected for reddening, while the data in the temperature-$(U-V)$ plot were shifted horizontally to force the cooler stars ($\log T_{\rm eff} \leq 4$) to superimpose to the theoretical ZAHB. In any case, what matters here is the trend of temperature with color, which is not altered by this zero-point correction.

The temperature-$(U-V)$ relation of ω Cen stars cannot be directly compared to the standard theoretical ZAHB, shown as a solid grey curve. This is because the U filter used by Bellini et al. (2009) differs substantially from the standard U band in the Johnson system (Momany et al. 2003, see discussion and Fig. 3). Hence, we re-computed the color – $T_{\rm eff}$ transformations

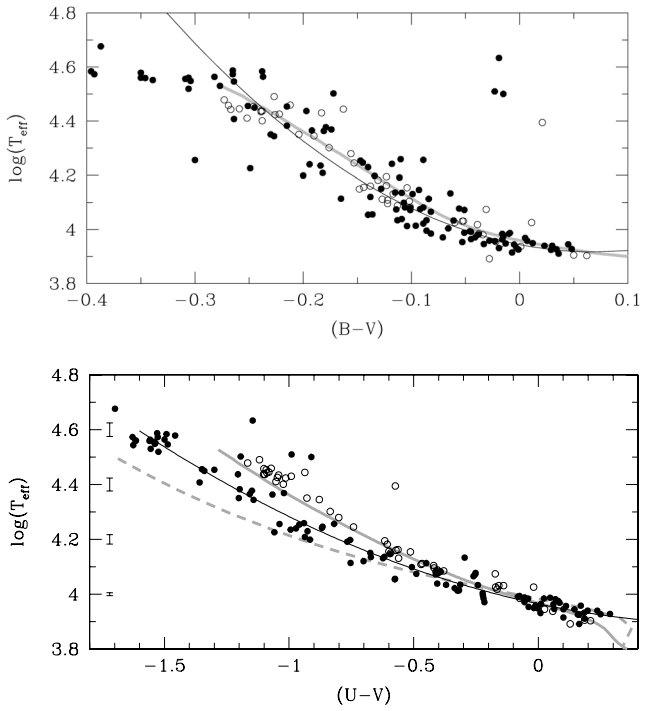

Fig. 14. Photometric color of the program stars as function of their measured temperature (filled circles). The black curve indicates the fit of the data, Eqs. (3 and (4). The grey thick curve shows the theoretical zero-age HB of Cassisi et al. (2009). The same model, re-derived for the non-standard filters used in the adopted photometry, is shown with a dashed grey curve. Empty circles show the position of NGC 6752 stars (Moni Bidin et al. 2007).

by adopting the transmission curve of the WFI@2.2 m non-standard U filter, following the same approach used in Momany et al. (2003) and applied these transformations to the stellar models by Pietrinferni et al. (2006). The ZAHB sequence transferred from the theoretical HR diagram to the observational one by using the appropriate set of transformations is shown as a grey dashed line in the central panel of Fig. 14.

The observed color–temperature distribution of target stars in NGC 6752 follows closely the theoretical ZAHB model, both in the upper and lower panels of Fig. 14. A similar agreement is observed for stars in M 80 and NGC 5986, using the spectroscopic temperatures of Moni Bidin et al. (2009) and the colors of Momany et al. (2003) and Momany et al. (2004), after correction of a photometric zero-point offset. The same trend is found for ω Cen stars, when the $(B - V)$ color is involved. However, the agreement between the ZAHB sequence transferred in the observational photometric plane with the appropriate transformations and observed $(U - V)$-temperature relation is limited only to $T_{\rm eff} \leq 12\,000$ K in this cluster. For hotter stars, the temperatures predicted by the model are lower than the ones we derive, and the difference increases monotonically, reaching up to ~8000 K at $T_{\rm eff} \approx 32\,000$ K.

The trend of reddening with temperature (discussed in Sect. 4.2) is too small to account for the disagreement between observed data and the re-calculated ZAHB model. Similarly, the assumed $E(U - V)$ cannot be the cause of the disagreement, since it can only shift horizontally the distribution of the data points. We also verified whether a reddening correction depending on the stellar $T_{\rm eff}$ value could, at least partially, account for the mismatch between theory and observations. For this aim, we adopted the approach outlined in Bedin et al. (2009). However, due to the not large (average) reddening of ω Cen, accounting for a reddening correction that depends on the $T_{\rm eff}$ would affect the theoretical prediction on the $(U - V)$ color at the level of a negligible ~0.02 mag.

Not even the temperature offset discussed in Sect. 4.1 can account for the disagreement between the observed and theoretical temperature-$(U - V)$ relation. Indeed, the use of different model spectra introduces only a too small offset (~400 K), which anyway shows a constant trend with temperature. On the other hand, the mismatch between the temperatures of our hottest targets and those derived by Moehler et al. (2011) is of the same order of their offset with respect to the theoretical temperature-color relation. However, Moehler et al.'s temperature estimates excellently agree with ours for stars cooler than 20 000 K, where the offset in Fig. 14 is clear. Moreover, a temperature offset would also affect the $T_{\rm eff} - (B - V)$ relation, contrary to what was observed. It might also affect NGC 6752 stars, because Moni Bidin et al. (2007) employed the same models used in this study.

It is quite natural to attribute the mismatch to the onset of atmospheric diffusion at 11 000–12 000 K (Grundahl et al. 1999), which alters the surface abundance of HB stars. Nevertheless, this interpretation presents a series of problems. First, the difference between the measured temperatures and the theoretical model does not follow the trend of the diffusion discussed in Sect. 4.3, which reaches a maximum at about 15 000 K and then fades out at higher temperatures. In addition, we checked the impact of diffusive processes on the location of the theoretical ZAHB locus in the $T_{\rm eff} - (U - V)$ plane. This was done by following the approach used in Dalessandro et al. (2011): we mimic the effect of diffusive processes by applying bolometric corrections appropriate for solar iron abundance when $T_{\rm eff}$ is larger than 12 000 K. However, we find that, at least for the $(U - V)$ color, the impact of diffusive processes on the predicted $T_{\rm eff}$-color relation is quite negligible, i.e., the ZAHB loci transferred in the observational plane by accounting (or not) for the occurrence of diffusive processes overlap almost perfectly. Finally, diffusion and radiative levitation are obviously also active in HB stars of NGC 6752 (Moehler et al. 2000; Moni Bidin et al. 2007), but they behave very differently.

One cannot exclude that the mismatch is simply due to a systematic introduced by the use of a non-standard U-filter. If this is the case, then even the presumably simple photometric calibration process might hide some unexpected results. In Momany et al. (2003) it was shown that the use of a slightly bluer U-filter (with respect to the standard one, see their Fig. 3) triggers the onset of an unphysical phenomenon: HB stars bluer than the instability strip can display $(U - B)$ colors redder than that of red giants at the same luminosity level. Indeed, the non-standard U-filter employed in the ω Cen data set, reduced first by Momany et al. (2003) and later by Bellini et al. (2009), covers a bluer wavelength range and misses almost completely the Balmer jump. This was shown to imply a fainter U-magnitude for the blue HB stars, which translated to redder $(U - B)$ colors (the so-called "BHB red incursion" Momany et al. 2003; or "ultraviolet deficiency" as in Markov et al. 2001). We verified that the observed $T_{\rm eff} - (U - V)$ relation is identical when the Bellini et al. (2009) photometric data are replaced with magnitudes from the Momany et al. (2003) catalog, except for a zero-point offset of about ≈0.1 mag, which only causes a horizontal shift of the points in Fig. 14. This behavior is not surprising, since the photometric calibration of Bellini et al. (2009) was performed by means of the Stetson (2000, 2005) secondary standards except for the U-filter, which was calibrated using the Momany et al. (2003) catalog, anchored to the Landolt (1992) system of standards.

The unavoidable conclusion is that the hottest stars in ω Cen are fainter than expectations in the U band. In fact, if a similar effect was also present in another band, or if the temperatures were overestimated, or if the stars were really hotter than expected, this would have been easily detected in the study of the reddening in Sect. 4.2 and in the $(B-V)$-temperature relation. A similar conclusion was reached for the blue HB at the level of the Grundahl et al. (1999) jump, and this feature was successfully correlated to the use of non-standard U-filters. We cannot draw a similar solid conclusion for the hottest ω Cen stars nor totally exclude that this is yet another new peculiarity of the ω Cen endless puzzle. In any case, the connection of this effect with the anomalous results discussed in Paper I is not straightforward, even if a temperature hotter than expectations could indeed explain both the observed offset in the temperature-gravity plane and the underestimated masses. More investigation is needed to find a comprehensive explanation of all these observations.

Before closing this section, we wish to note that since ω Cen hosts a stellar sub-population hugely enhanced in He abundance (see King et al. 2012, and references therein), one has to check if the disagreement between the location of the GC hot HB stars with respect the theoretical ZAHB computed by accounting for a canonical He abundance could be partially accounted for by considering a ZAHB locus corresponding to an He-enhanced stellar population. We verified this scenario by comparing a ZAHB locus for $Y = 0.40$ with the empirical data. However, at the cooler $T_{\rm eff}$ values where the He-enhanced ZAHB is redder than the ZAHB for the canonical He content, the two ZAHBs overlap almost perfectly in the hot temperature regime. As a consequence, the occurrence of the multiple population phenomenon in ω Cen cannot help in solving the observed discrepancy between theory and observations.

5. Conclusions

We analyzed the fundamental parameters spectroscopically derived for a sample of more than 100 HB stars in ω Cen. Our results can be summarized as follows:

- We showed that the surface helium abundances measured on low-resolution spectra are systematically higher by about 0.2−0.25 dex with respect to measurements at higher resolution. The presence of this offset was already suspected in previous works.
- We derived a mean cluster reddening of $E(B-V) = 0.115 \pm 0.004$, in good agreement with previous estimates. However, we confirmed the recent discovery by Calamida et al. (2005) that the reddening is not uniform across the cluster area, with our measurements being on average 0.03−0.04 mag higher in the western half than in the southeast region.
- The surface helium abundance of ω Cen HB stars hotter than 11 500 K is very similar to that of analogous stars in other clusters, despite their peculiar gravity discovered by Moni Bidin et al. (2011a). Diffusion processes efficiently erase the differences among the atmospheres of stars with different initial chemical composition. From the measurements of 121 stars in four clusters, we find a clear trend of surface helium with temperature, which most probably reflects a dependence of diffusion efficiency with temperature. In fact, the helium abundance decreases with $T_{\rm eff}$, reaching a minimum at ∼15 000 K and then increases again for hotter stars.
- The surface helium abundance of EHB stars mildly increases with temperature for $T_{\rm eff} \geq 27\,000$ K, analogous to the trend observed among field stars, but the measurements are more scattered than what would be expected for observational errors alone. In both ω Cen and NGC 6752, where a significant sample was analyzed (≥14 targets), ∼15% of the EHB stars have a surface helium abundance ∼1 dex lower than the others. This suggests that two families of EHB stars with different helium abundances are present even in GCs, analogous to what Edelmann et al. (2003) observed among field objects. However, evidence that our EHB stars follow a bimodal distribution is still not conclusive because it is blurred by observational errors.
- Two groups of BH candidate stars are observed in our sample: the majority has a solar or super-solar surface helium abundance, while a small quantity (14%) is strongly helium depleted ($\log(N({\rm He})/N({\rm H})) \leq -2$). This result confirms what had already been found by previous investigations, both in ω Cen (Moehler et al. 2011) and in the field (Edelmann et al. 2003). However, we detect a fraction of helium-poor objects lower than what had been previously measured. This lower fraction cannot be due to a different definition of the transition between the two groups or by the aforementioned offset in helium abundance because the gap between the two groups is very large (≥1 dex). Our results are consistent with the scenario where the helium-depleted BH candidates are post-HB objects evolving off toward the white dwarf cooling sequence, as proposed by Moehler et al. (2011).
- We do not detect an asymmetric spatial distribution of helium-rich BH stars, at variance with Moehler et al. (2011). Nevertheless, the helium-poor objects are more frequent in the southeast half by about a factor of three, both in our and their sample. This finding is not affected by the non-uniform cluster sampling, which could be introducing selection effects when the spatial distribution of BH stars is analyzed. However, the result is only marginally significative, because a Kolmogorov-Smirnov test revealed that it has a 10% probability of being due to pure chance only.
- We find indications that EHB stars with anomalously high spectroscopic mass could be present even in ω Cen after their discovery in NGC 6752 and M 80 (Moni Bidin et al. 2007, 2009). Their fraction is lower than in the other clusters, but the difference is not significative. Their photometric behavior resembles that of their analogs in the other clusters. Unfortunately, only three such stars are detected, too few for a more detailed analysis of their properties.
- Our targets follow a $(B-V)-T_{\rm eff}$ relation that is well reproduced by the theoretical HB models. The empirical $(U-V)-T_{\rm eff}$ curve, on the contrary, matches the models only for $T_{\rm eff} \leq 11\,000$ K, hotter stars being systematically redder than the theoretical expectations. HB stars in NGC 6752 do not deviate from the model curve. This cannot be explained by diffusion processes alone and points to another peculiarity of ω Cen HB stars, in addition to those already discussed by Moni Bidin et al. (2011a), with respect to their analogs in NGC 6752 and other two comparison clusters. We do not have an explanation for this behavior.

Acknowledgements. C.M.B. acknowledges support by the FONDAP Center for Astrophysics 15010003, BASAL Center for Astrophysics and Associated Technologies (CATA) PFB-06/2007. S.C. is grateful for financial support from PRIN-INAF 2009 "Formation and Early Evolution of Massive Star Clusters" (PI: R. Gratton) and PRIN-INAF 2011 "Multiple populations in Globular Clusters: their role in the Galaxy assembly" (PI: E. Carretta).

References

Baschek, B. 1975, Abundance anomalies in early-type stars, eds. B. Baschek, W. H. Kegel, & G. Traving, 101
Bedin, L. R., Piotto, G., Anderson, J., et al. 2004, ApJ, 605, L125
Bedin, L. R., Salaris, M., Piotto, G., et al. 2009, ApJ, 697, 965
Behr, B. B. 2003, ApJS, 149, 67
Bellini, A., Piotto, G., Bedin, L. R., et al. 2009, A&A, 493, 959
Bellini, A., Bedin, L. R., Piotto, G., et al. 2010, AJ, 140, 631
Bergeron, P., Saffer, R. A., & Liebert, J. 1992, ApJ, 394, 228
Binney, J., & Merrifield, M. 1998, Galactic Astronomy (Princeton, NJ: Princeton University Press)
Brown, T. M., Sweigart, A. V., Lanz, T., Landsman, W. B., & Hubeny, I. 2001, ApJ, 562, 368
Busso, G., Cassisi, S., Piotto, G., et al. 2007, A&A, 474, 105
Calamida, A., Stetson, P. B., Bono, G., et al. 2005, ApJ, 634, L69
Cardelli, J. A., Clayton, G. C., & Mathis, J. S. 1989, ApJ, 345, 245
Cassisi, S., Schlattl, H., Salaris, M., & Weiss, A. 2003, ApJ, 582, L43
Cassisi, S., Salaris, M., Anderson, J., et al. 2009, ApJ, 702, 1530
Castellani, M., & Castellani, V. 1993, ApJ, 407, 649
Castellani, V., Calamida, A., Bono, G., et al. 2007, ApJ, 663, 1021
Catelan, M. 2009, Ap&SS, 320, 261
Dalessandro, E., Salaris, M., Ferraro, F. R., et al. 2011, MNRAS, 410, 694
D'Antona, F., Caloi, V., Montalbán, J., Ventura, P., & Gratton, R. 2002, A&A, 395, 69
D'Antona, F., Bellazzini, M., Caloi, V., et al. 2005, ApJ, 631, 868
D'Antona, F., Caloi, V., & Ventura, P. 2010, MNRAS, 405, 2295
D'Cruz, N. L., Dorman, B., Rood, R. T., & O'Connell, R. W. 1996, ApJ, 466, 359
D'Cruz, N. L., O'Connell, R. W., Rood, R. T., et al. 2000, ApJ, 530, 352
Dotter, A., Sarajedini, A., Anderson, J., et al. 2010, ApJ, 708, 698
Edelmann, H., Heber, U., Hagen, H.-J., et al. 2003, A&A, 400, 939
Fabbian, D., Recio-Blanco, A., Gratton, R. G., & Piotto, G. 2005, A&A, 434, 235
Faulkner, J. 1966, ApJ, 144, 978
Flower, P. J. 1996, ApJ, 469, 355
Fraix-Burnet, D., Davoust, E., & Charbonnel, C. 2009, MNRAS, 398, 1706
Fusi Pecci, F., Ferraro, F. R., Bellazzini, M., et al. 1993, AJ, 105, 1145
Glaspey, J. W., Michaud, G., Moffat, A. F. J., & Demers, S. 1989, ApJ, 339, 926
Gratton, R. G., Carretta, E., Bragaglia, A., Lucatello, S., & D'Orazi, V. 2010, A&A, 517, A81
Grebel, E. K., & Roberts, W. J. 1995, A&AS, 109, 293
Greenstein, G. S. 1967, Nature, 213, 871
Grundahl, F., Catelan, M., Landsman, W. B., Stetson, P. B., & Andersen, M. I. 1999, ApJ, 524, 242
Hamuy, M., Walker, A. R., Suntzeff, N. B., et al. 1992, PASP, 104, 533
Harris, W. E. 1996, AJ, 112, 1487
Heber, U. 1987, Mitteilungen der Astronomischen Gesellschaft Hamburg, 70, 79
Hirsch, H. A., Heber, U., & O'Toole, S. J. 2008, in Hot Subdwarf Stars and Related Objects, eds. U. Heber, C. S. Jeffery, & R. Napiwotzki, ASP Conf. Ser., 392, 131
Hoyle, F., & Schwarzschild, M. 1955, ApJS, 2, 1
Hubeny, I., & Lanz, T. 1995, ApJ, 439, 875
King, I. R., Bedin, L. R., Cassisi, S., et al. 2012, AJ, 144, 5
Kurucz, R. 1993, ATLAS9 Stellar Atmosphere Programs and 2 km s^{-1} grid, Kurucz CD-ROM No. 13 (Cambridge, Mass.: Smithsonian Astrophysical Observatory)
Landolt, A. U. 1992, AJ, 104, 340
Lanz, T., & Hubeny, I. 2003, ApJS, 146, 417
Lanz, T., & Hubeny, I. 2007, ApJS, 169, 83
Lanz, T., Brown, T. M., Sweigart, A. V., Hubeny, I., & Landsman, W. B. 2004, ApJ, 602, 342
Lee, Y., Joo, S., Han, S., et al. 2005, ApJ, 621, L57
Lisker, T., Heber, U., Napiwotzki, R., et al. 2005, A&A, 430, 223
Lub, J. 2002, in Omega Centauri, A Unique Window into Astrophysics, eds. F. van Leeuwen, J. D. Hughes, & G. Piotto, ASP Conf. Ser., 265, 95
Markov, H. S., Spassova, N. M., & Baev, P. V. 2001, MNRAS, 326, 102
Michaud, G., Vauclair, G., & Vauclair, S. 1983, ApJ, 267, 256
Michaud, G., Richer, J., & Richard, O. 2008, ApJ, 675, 1223
Milone, A. P., Piotto, G., King, I. R., et al. 2010, ApJ, 709, 1183
Moehler, S., Sweigart, A. V., & Catelan, M. 1999, A&A, 351, 519
Moehler, S., Sweigart, A. V., Landsman, W. B., & Heber, U. 2000, A&A, 360, 120
Moehler, S., Landsman, W. B., Sweigart, A. V., & Grundahl, F. 2003, A&A, 405, 135
Moehler, S., Sweigart, A. V., Landsman, W. B., Hammer, N. J., & Dreizler, S. 2004, A&A, 415, 313
Moehler, S., Dreizler, S., Lanz, T., et al. 2011, A&A, 526, A136
Momany, Y., Piotto, G., Recio-Blanco, A., et al. 2002, ApJ, 576, L65
Momany, Y., Cassisi, S., Piotto, G., et al. 2003, A&A, 407, 303
Momany, Y., Bedin, L. R., Cassisi, S., et al. 2004, A&A, 420, 605
Moni Bidin, C., & Piotto, G. 2010, Ap&SS, 329, 19
Moni Bidin, C., Moehler, S., Piotto, G., et al. 2006, A&A, 451, 499
Moni Bidin, C., Moehler, S., Piotto, G., Momany, Y., & Recio-Blanco, A. 2007, A&A, 474, 505
Moni Bidin, C., Moehler, S., Piotto, G., Momany, Y., & Recio-Blanco, A. 2009, A&A, 498, 737
Moni Bidin, C., Villanova, S., Piotto, G., Moehler, S., & D'Antona, F. 2011a, ApJ, 738, L10
Moni Bidin, C., Villanova, S., Piotto, G., & Momany, Y. 2011b, A&A, 528, A127
Morse, J. A., Mathieu, R. D., & Levine, S. E. 1991, AJ, 101, 1495
Napiwotzki, R. 1997, A&A, 322, 256
Napiwotzki, R., Green, P. J., & Saffer, R. A. 1999, ApJ, 517, 399
O'Toole, S. J. 2008, in Hot Subdwarf Stars and Related Objects, eds. U. Heber, C. S. Jeffery, & R. Napiwotzki, ASP Conf. Ser., 392, 67
Pace, G., Recio-Blanco, A., Piotto, G., & Momany, Y. 2006, A&A, 452, 493
Peacock, J. A. 1983, MNRAS, 202, 615
Peterson, R. C. 1983, ApJ, 275, 737
Pietrinferni, A., Cassisi, S., Salaris, M., & Castelli, F. 2006, ApJ, 642, 797
Piotto, G., Zoccali, M., King, I. R., et al. 1999, AJ, 118, 1727
Piotto, G., Villanova, S., Bedin, L. R., et al. 2005, ApJ, 621, 777
Piotto, G., Bedin, L. R., Anderson, J., et al. 2007, ApJ, 661, L53
Quievy, D., Charbonneau, P., Michaud, G., & Richer, J. 2009, A&A, 500, 1163
Recio-Blanco, A., Aparicio, A., Piotto, G., de Angeli, F., & Djorgovski, S. G. 2006, A&A, 452, 875
Ripepi, V., Clementini, G., Di Criscienzo, M., et al. 2007, ApJ, 667, L61
Rosenberg, A., Recio-Blanco, A., & García-Marín, M. 2004, ApJ, 603, 135
Saffer, R. A., Bergeron, P., Koester, D., & Liebert, J. 1994, ApJ, 432, 351
Sandage, A., & Wildey, R. 1967, ApJ, 150, 469
Scarpa, R., & Falomo, R. 2010, A&A, 523, A43
Sollima, A., Pancino, E., Ferraro, F. R., et al. 2005, ApJ, 634, 332
Stetson, P. B. 2000, PASP, 112, 925
Stetson, P. B. 2005, PASP, 117, 563
Ströer, A., Heber, U., Lisker, T., Napiwotzki, R., & Dreizler, S. 2005, in 14th European Workshop on White Dwarfs, eds. D. Koester, & S. Moehler, ASP Conf. Ser., 334, 309
Sweigart, A. V. 1997, ApJ, 474, L23
Tonry, J., & Davis, M. 1979, AJ, 84, 1511
van de Ven, G., van den Bosch, R. C. E., Verolme, E. K., & de Zeeuw, P. T. 2006, A&A, 445, 513
van den Bergh, S. 1967, AJ, 72, 70
Villanova, S., Piotto, G., & Gratton, R. G. 2009, A&A, 499, 755
Villanova, S., Geisler, D., Piotto, G., & Gratton, R. 2012, ApJ, 748, 62
Werner, K. 1996, ApJ, 457, L39
Werner, K., & Dreizler, S. 1999, J. Comput. Appl. Math., 109, 65
Whitney, J. H., Rood, R. T., O'Connell, R. W., et al. 1998, ApJ, 495, 284

Pages 13 to 14 are available in the electronic edition of the journal at http://www.aanda.org

Table 2. Derived parameters of the target stars.

ID	V	$(U-V)$	$(B-V)$	$T_{\rm eff}$ K	$\log(g)$ dex	$\log\left(\frac{N(\rm He)}{N(\rm H)}\right)$ dex	M $M_\odot$	$E(B-V)$	$\rm RV_H$ km s^{-1}	Notes
75369	15.285	−0.048	0.054	10 800 ± 130	3.36 ± 0.06	–	0.27 ± 0.03	0.140	228	
75469	15.437	−0.066	0.033	11 600 ± 120	3.76 ± 0.03	−2.10 ± 0.54	0.52 ± 0.05	0.130	236	
76912	15.687	−0.295	0.001	11 900 ± 180	3.60 ± 0.03	−2.05 ± 0.51	0.28 ± 0.03	0.106	224	
77018	15.647	−0.255	0.031	13 000 ± 160	3.92 ± 0.03	−2.05 ± 0.27	0.52 ± 0.05	0.150	288	M
77151	15.149	0.139	0.064	9730 ± 40	3.30 ± 0.06	–	0.33 ± 0.03	0.106	214	
77359	14.871	0.431	0.145	8700 ± 40	3.09 ± 0.06	–	0.35 ± 0.04	0.136	288	
77547	14.995	0.279	0.120	9300 ± 60	3.22 ± 0.03	–	0.35 ± 0.03	0.144	223	
78728	15.469	−0.209	0.023	11 900 ± 200	3.73 ± 0.06	−2.08 ± 0.60	0.46 ± 0.06	0.125	248	
79423	15.442	−0.197	0.026	12 100 ± 200	3.65 ± 0.06	−2.56 ± 0.78	0.38 ± 0.05	0.133	189	
79535	14.730	0.482	0.163	8470 ± 60	2.97 ± 0.09	–	0.33 ± 0.04	0.142	228	
79548	16.260	−0.572	0.004	15 500 ± 200	4.18 ± 0.03	−2.04 ± 0.15	0.39 ± 0.04	0.157	222	
81127	15.312	−0.059	0.064	11 800 ± 120	3.79 ± 0.03	−1.57 ± 0.24	0.61 ± 0.06	0.164	267	
81531	18.464	−1.335	−0.150	38 700 ± 300	5.67 ± 0.06	−1.02 ± 0.06	0.36 ± 0.04	0.146	236	M
82039	15.824	−0.423	0.000	13 700 ± 180	4.00 ± 0.03	−1.76 ± 0.18	0.48 ± 0.05	0.131	291	
82876	16.055	−0.429	0.016	13 500 ± 200	3.91 ± 0.03	−2.11 ± 0.36	0.32 ± 0.03	0.145	305	
83092	14.968	0.255	0.099	9180 ± 40	3.10 ± 0.09	–	0.28 ± 0.04	0.122	289	
84344	14.846	0.392	0.138	8700 ± 70	3.00 ± 0.06	–	0.29 ± 0.03	0.133	279	
84407	14.905	0.217	0.105	9650 ± 30	3.27 ± 0.06	–	0.39 ± 0.04	0.144	232	
85323	17.128	−0.732	−0.025	17 000 ± 300	4.76 ± 0.12	−2.15 ± 0.12	0.57 ± 0.09	0.132	246	M
85415	15.033	0.241	0.106	9700 ± 50	3.31 ± 0.06	–	0.38 ± 0.04	0.147	302	
85568	15.029	0.274	0.100	9440 ± 50	3.26 ± 0.15	–	0.36 ± 0.06	0.130	231	
86663	15.202	0.153	0.099	9640 ± 50	3.19 ± 0.09	–	0.25 ± 0.03	0.141	263	
87776	17.806	−1.008	−0.115	22 400 ± 400	5.09 ± 0.03	−1.87 ± 0.09	0.38 ± 0.04	0.090	205	
88234	15.815	−0.313	0.008	12 500 ± 140	3.81 ± 0.06	−2.20 ± 0.39	0.36 ± 0.04	0.122	224	
89168	15.291	−0.119	0.029	10 800 ± 170	3.27 ± 0.09	–	0.22 ± 0.03	0.117	222	
89638	18.547	−1.306	−0.122	36 600 ± 1000	5.66 ± 0.12	−0.21 ± 0.15	0.35 ± 0.06	0.165	231	M
90381	14.891	0.364	0.122	9070 ± 50	3.16 ± 0.18	–	0.36 ± 0.07	0.136	249	
91164	18.577	−1.330	−0.191	33 100 ± 1200	5.67 ± 0.09	−1.08 ± 0.18	0.39 ± 0.07	0.072	189	T
91573	18.313	−1.011	−0.082	27 400 ± 1800	5.61 ± 0.12	−2.69 ± 0.54	0.56 ± 0.16	0.148	210	M
91877	15.352	−0.029	0.049	10 090 ± 30	3.18 ± 0.12	–	0.19 ± 0.03	0.116	246	
92018	18.308	−1.146	−0.130	28 200 ± 1300	5.53 ± 0.12	−1.92 ± 0.15	0.44 ± 0.11	0.107	206	T
93131	17.531	−0.778	−0.079	17 400 ± 500	4.73 ± 0.12	−1.67 ± 0.18	0.35 ± 0.06	0.083	172	
93226	16.215	−0.561	−0.019	15 800 ± 400	4.14 ± 0.09	−2.35 ± 0.27	0.36 ± 0.06	0.137	251	
94034	14.957	0.305	0.092	9050 ± 30	3.11 ± 0.15	–	0.30 ± 0.05	0.106	217	
95259	15.934	−0.401	0.022	14 000 ± 300	3.98 ± 0.09	−2.66 ± 0.03	0.40 ± 0.06	0.158	210	
95987	18.364	−1.106	−0.100	28 400 ± 1200	5.47 ± 0.09	−2.24 ± 0.33	0.36 ± 0.08	0.139	180	T
96597	15.531	−0.218	0.009	12 100 ± 170	3.59 ± 0.06	−2.46 ± 0.99	0.30 ± 0.04	0.118	220	
97034	17.500	−0.827	−0.059	23 400 ± 1600	4.90 ± 0.15	−2.62 ± 0.36	0.30 ± 0.10	0.159	153	T
97088	16.109	−0.478	0.006	13 700 ± 300	3.74 ± 0.09	−2.02 ± 0.30	0.21 ± 0.03	0.140	206	
98189	18.434	−1.348	−0.194	36 000 ± 1000	5.89 ± 0.09	−0.92 ± 0.15	0.66 ± 0.10	0.086	209	T
98349	15.018	0.295	0.160	8820 ± 70	3.08 ± 0.21	–	0.29 ± 0.07	0.160	191	
98857	18.855	−1.342	−0.224	35 600 ± 900	5.83 ± 0.12	−0.62 ± 0.12	0.40 ± 0.07	0.053	200	
99148	14.914	0.378	0.112	8540 ± 70	2.92 ± 0.18	–	0.24 ± 0.05	0.100	204	
100171	18.900	−1.361	−0.162	33 900 ± 1700	5.73 ± 0.15	−0.23 ± 0.15	0.32 ± 0.08	0.106	230	M
100288	15.541	−0.204	0.014	12 000 ± 190	3.78 ± 0.12	−1.72 ± 0.36	0.47 ± 0.08	0.118	161	
100817	15.190	−0.058	0.059	12 000 ± 110	3.71 ± 0.09	−1.50 ± 0.30	0.56 ± 0.07	0.163	226	
101202	16.709	−0.625	0.026	18 000 ± 400	4.65 ± 0.09	−2.15 ± 0.21	0.59 ± 0.07	0.199	276	
101650	15.558	−0.217	0.014	11 800 ± 140	3.60 ± 0.09	−2.07 ± 0.48	0.31 ± 0.04	0.117	204	
102372	14.908	0.339	0.110	8800 ± 80	3.01 ± 0.24	–	0.27 ± 0.07	0.112	188	
103232	18.561	−1.293	−0.149	35 200 ± 600	5.49 ± 0.06	−0.83 ± 0.09	0.24 ± 0.03	0.132	224	
104153	16.090	−0.480	−0.013	14 200 ± 500	4.00 ± 0.12	−2.63 ± 0.75	0.36 ± 0.07	0.124	215	
104974	14.773	0.444	0.149	8450 ± 120	3.06 ± 0.21	–	0.39 ± 0.09	0.121	302	
105290	19.180	−1.252	−0.035	36 000 ± 2000	5.33 ± 0.07	+0.69 ± 0.42	0.12 ± 0.04	–	237	
105596	14.924	0.353	0.114	8430 ± 70	3.04 ± 0.09	–	0.33 ± 0.04	0.085	218	
107532	15.015	0.263	0.077	9590 ± 50	3.38 ± 0.15	–	0.46 ± 0.08	0.110	166	
106348	15.156	0.112	0.070	9810 ± 70	3.28 ± 0.09	–	0.31 ± 0.04	0.116	203	
108101	14.953	0.205	0.070	9220 ± 70	3.10 ± 0.12	–	0.28 ± 0.04	0.095	201	
108102	19.035	−1.333	−0.150	37 000 ± 3000	5.79 ± 0.33	+1.33 ± 0.24	0.29 ± 0.13	0.142	233	
108309	18.629	−1.298	−0.123	38 300 ± 900	5.85 ± 0.15	−0.71 ± 0.15	0.47 ± 0.09	0.172	228	
109104	14.985	0.119	0.069	9860 ± 70	3.27 ± 0.18	–	0.35 ± 0.07	0.117	288	
109474	16.806	−0.672	−0.030	17 600 ± 400	4.40 ± 0.09	−1.85 ± 0.12	0.31 ± 0.05	0.145	225	
113991	18.357	−1.502	−0.243	64 000 ± 13 000	5.77 ± 0.15	−0.09 ± 0.42	0.28 ± 0.23	–	263	
114321	16.643	−0.746	0.005	18 200 ± 400	4.35 ± 0.09	−1.66 ± 0.12	0.30 ± 0.05	0.187	268	
114375	16.888	−0.674	−0.003	17 400 ± 400	4.68 ± 0.09	−1.86 ± 0.18	0.56 ± 0.09	0.162	255	
128044	14.923	0.258	0.082	8840 ± 30	3.12 ± 0.09	–	0.34 ± 0.04	0.082	219	

Table 2. continued.

ID	V	$(U-V)$	$(B-V)$	$T_{\rm eff}$	$\log(g)$	$\log\left(\frac{N(\rm He)}{N(\rm H)}\right)$	M	$E(B-V)$	$\rm RV_H$	Notes
129495	15.018	0.358	0.345	7800 ± 50	3.04 ± 0.15	–	0.41 ± 0.07	0.233	191	
131429	15.435	−0.176	0.002	10 810 ± 70	3.67 ± 0.09	–	0.48 ± 0.06	0.081	304	
132039	15.419	−0.130	0.011	10 290 ± 40	3.42 ± 0.09	–	0.30 ± 0.04	0.080	288	
133061	15.217	−0.102	0.051	13 600 ± 200	3.90 ± 0.12	−2.75 ± 0.48	0.68 ± 0.11	0.182	191	
133073	15.033	0.176	0.127	8900 ± 80	3.15 ± 0.21	–	0.33 ± 0.07	0.130	240	
133686	14.796	0.192	0.102	8880 ± 20	3.11 ± 0.15	–	0.37 ± 0.06	0.105	268	
133674	14.994	0.203	0.096	8540 ± 60	3.07 ± 0.09	–	0.32 ± 0.04	0.075	249	
134857	14.858	0.295	0.108	8200 ± 150	3.07 ± 0.09	–	0.41 ± 0.06	0.054	204	
136031	15.026	0.183	0.087	9090 ± 40	3.14 ± 0.15	–	0.30 ± 0.05	0.103	196	
136206	14.855	0.358	0.144	8410 ± 90	3.11 ± 0.06	–	0.42 ± 0.05	0.108	239	
137401	15.084	0.155	0.062	8980 ± 50	3.03 ± 0.12	–	0.23 ± 0.03	0.076	288	
137858	14.715	0.380	0.151	8100 ± 100	2.93 ± 0.12	–	0.35 ± 0.05	0.097	200	
131319	15.217	−0.022	0.044	9340 ± 60	3.14 ± 0.12	–	0.24 ± 0.04	0.074	250	
133035	14.899	0.139	0.074	9360 ± 50	3.20 ± 0.18	–	0.36 ± 0.07	0.103	182	
133511	15.296	−0.028	0.029	9890 ± 70	3.42 ± 0.15	–	0.37 ± 0.06	0.073	209	
133767	15.584	−0.381	−0.021	11 400 ± 170	3.36 ± 0.12	–	0.19 ± 0.03	0.078	226	
134888	15.386	−0.142	0.026	10 500 ± 110	3.49 ± 0.18	–	0.35 ± 0.07	0.101	160	
135572	15.992	−0.559	−0.050	13 000 ± 300	3.87 ± 0.09	−2.24 ± 0.54	0.33 ± 0.05	0.071	230	M
135942	15.924	−0.507	−0.023	13 200 ± 180	3.96 ± 0.09	−2.77 ± 0.60	0.43 ± 0.06	0.099	216	
136852	15.427	−0.124	0.019	10 340 ± 50	3.40 ± 0.12	–	0.28 ± 0.04	0.091	242	
137998	15.686	−0.382	−0.025	11 300 ± 140	3.38 ± 0.09	–	0.18 ± 0.02	0.072	206	
141523	15.574	−0.212	0.006	10 900 ± 190	3.55 ± 0.12	–	0.32 ± 0.05	0.091	123	
144281	15.328	−0.026	0.033	9650 ± 50	3.32 ± 0.18	–	0.30 ± 0.06	0.071	248	
154412	17.863	−1.422	−0.235	36 300 ± 200	5.30 ± 0.06	−0.99 ± 0.09	0.29 ± 0.03	0.054	232	
156638	18.680	−1.504	−0.272	47 000 ± 3000	5.57 ± 0.06	−2.24 ± 0.39	0.18 ± 0.04	0.042	280	
157531	18.277	−0.952	0.096	43 000 ± 800	5.46 ± 0.03	−0.90 ± 0.18	0.23 ± 0.03	0.402	223	
166106	19.127	−1.431	−0.399	35 000 ± 800	5.59 ± 0.09	−0.70 ± 0.12	0.18 ± 0.03	−0.121	223	T
167821	18.754	−1.434	−0.278	37 400 ± 500	5.72 ± 0.06	−1.02 ± 0.06	0.32 ± 0.04	0.014	247	
172573	16.538	−0.722	−0.085	15 800 ± 300	4.24 ± 0.06	−2.13 ± 0.18	0.34 ± 0.04	0.070	260	
173876	17.685	−0.955	−0.064	23 800 ± 500	5.04 ± 0.09	−2.33 ± 0.15	0.34 ± 0.05	0.154	262	T
174767	16.836	−0.865	−0.134	16 800 ± 300	4.39 ± 0.03	−1.88 ± 0.12	0.32 ± 0.04	0.031	245	
175847	18.547	−1.263	−0.235	37 900 ± 900	5.82 ± 0.12	−0.59 ± 0.12	0.48 ± 0.08	0.059	264	
178139	18.078	−0.796	0.092	32 300 ± 600	5.47 ± 0.06	−0.96 ± 0.12	0.40 ± 0.05	0.356	257	
180700	17.444	−0.844	−0.185	18 000 ± 400	4.65 ± 0.06	−2.15 ± 0.18	0.29 ± 0.04	−0.012	275	
181428	18.851	−1.620	−0.281	38 400 ± 1600	5.85 ± 0.09	−2.63 ± 0.33	0.38 ± 0.08	0.014	308	
183124	18.006	−0.717	0.100	31 700 ± 900	5.36 ± 0.06	−1.79 ± 0.15	0.34 ± 0.05	0.366	209	T
224916	18.530	−1.421	−0.191	36 300 ± 800	5.77 ± 0.09	−0.50 ± 0.09	0.46 ± 0.07	0.093	223	
225063	18.692	−1.366	−0.231	36 200 ± 600	5.72 ± 0.06	−0.74 ± 0.06	0.35 ± 0.04	0.053	258	
225931	17.101	−0.800	−0.069	17 200 ± 300	4.51 ± 0.06	−1.65 ± 0.09	0.32 ± 0.04	0.097	269	
229084	18.171	−1.155	−0.136	28 600 ± 700	5.59 ± 0.12	−2.19 ± 0.18	0.57 ± 0.10	0.101	245	M,T
229880	16.801	−0.765	−0.032	17 900 ± 400	4.46 ± 0.06	−1.81 ± 0.15	0.35 ± 0.05	0.145	231	
230786	17.993	−1.000	−0.057	31 800 ± 700	5.65 ± 0.06	−1.50 ± 0.09	0.66 ± 0.09	0.203	203	T
232593	18.429	−1.364	−0.167	36 600 ± 900	5.73 ± 0.09	−0.55 ± 0.12	0.45 ± 0.07	0.119	214	
232682	17.262	−0.948	−0.112	22 100 ± 500	4.87 ± 0.09	−1.93 ± 0.09	0.39 ± 0.06	0.096	205	T
233133	17.457	−1.004	−0.100	24 100 ± 600	5.04 ± 0.06	−2.30 ± 0.15	0.41 ± 0.06	0.121	209	M,T
234000	16.650	−0.743	−0.067	16 200 ± 400	4.31 ± 0.09	−1.76 ± 0.12	0.34 ± 0.06	0.091	255	M
234333	17.802	−1.345	−0.189	35 300 ± 800	5.30 ± 0.06	−2.35 ± 0.30	0.31 ± 0.04	0.096	241	M
235103	17.524	−0.964	−0.077	23 200 ± 600	4.74 ± 0.15	−1.71 ± 0.12	0.21 ± 0.04	0.143	236	T
236142	17.888	−1.165	−0.149	25 600 ± 600	5.22 ± 0.06	−3.37 ± 0.18	0.37 ± 0.05	0.076	212	T
236428	17.609	−0.873	−0.066	23 100 ± 700	5.08 ± 0.12	−3.26 ± 0.15	0.42 ± 0.08	0.145	199	T